

Ground-penetrating Radar and Geoelectrical Simulations of Data from the Floridablanca Archaeological Site

M. DE LA VEGA,^{1,*} A. OSELLA,¹ E. LASCANO¹ AND J. M. CARCIONE²

¹ Dto. de Física-Facultad de Ciencias Exactas y Naturales-Universidad de Buenos Aires, Ciudad Universitaria, Pab. 1, 1428, Buenos Aires, Argentina

² Istituto Nazionale di Oceanografia e di Geofisica Sperimentale (OGS), Borgo Grotta Gigante 42c, 34010 Sgonico, Trieste-Italy

ABSTRACT In this work we characterize the electromagnetic response of archaeological remains of a Spanish fortress situated on the Atlantic coast in Patagonia (Argentina). The fortress, part of the Floridablanca colony, founded in the eighteenth century, has been surveyed with non-invasive electromagnetic techniques (ground-penetrating radar (GPR) and the geo-electric method). The surveys indicate the presence of adobe walls of various sizes and width having different preservation states. Use of inversion algorithms alone to interpret the data has not been conclusive in obtaining a reliable model, because many uncertainties remained. To aid the interpretation, we make use of modelling methods to simulate the low- and high-frequency electromagnetic responses of the structures. The walls can be differentiated in spite of the low resistivity contrast with the surrounding media. The resolution of the 500 MHz antenna allows a satisfactory determination of the location of the walls and their conservation state. Similarly, the geo-electrical response has enough sensitivity to detect the inner and major walls. Copyright © 2005 John Wiley & Sons, Ltd.

Key words: simulation; ground-penetrating radar; geo-electric; walls; resolution; Floridablanca

Introduction

Geophysical methods have proven to be very useful to archaeologists in order to detect, map and study the characteristics of different types of objects and structures in the subsurface. These methods allow the evaluation of their conservation state, the identification of different construction phases and zones disturbed by agricultural activities or plundering. Moreover, the investigation of geological deposits and buried landforms is useful for generating palaeoenvironmental

information (e.g. Herbich *et al.*, 1997; Silliman *et al.*, 2000; Weston, 2001). Although these methods have been applied systematically in archaeology during the past 50 years, their implementation in Argentina is relatively new, having started in the middle of the 1990s (Carrara, 1996; Ponti *et al.*, 1996).

In 2000, we started the acquisition of geophysical profiles at the Floridablanca archaeological site, which is located near San Julián Bay, Argentina. Floridablanca was a Spanish colony inhabited for a period of four years (1781–1784). The site has an area of 10 000 m² and is characterized by the presence of elevations of the terrain that correspond to buried archaeological structures, as indicated by previous excavations (Senatore *et al.*, 2000). The objective of the survey was to detect the buried

* Correspondence to: M. de la Vega, Dto. de Física-Facultad de Ciencias Exactas y Naturales-Universidad de Buenos Aires, Ciudad Universitaria, Pab. 1, 1428, Buenos Aires, Argentina.
E-mail: matias@df.uba.ar

structures (mostly adobe walls), delimit them, find their characteristics and study the presence of tiles due to roof collapse within the zone of interest.

Our study focused on two sectors of the site: North Wing I (NWI) and South Wing II (SWII; see Lascano *et al.* (2003), figure 3 and table 1 for a map of the site). According to the historical investigations, these sectors should correspond to settlers houses, but there is no information about the internal organization of the houses and their occupation before the abandonment of the colony (Senatore, 2000).

Archaeological excavations were carried out at both NWI and SWII, with only one house being dug in each sector. It is possible to determinate three types of walls on the basis of their width and construction characteristics. The three types of walls found are: (i) 0.8 m thick external walls, (ii) 0.45 m thick dividing walls between houses (separation walls) and (iii) 0.25 m thick inner walls. All the walls are made of adobe (clay brick).

The house excavated in the NWI sector presented no roof remains and a low artefact density. In contrast, in the SWII sector a roof collapse (tiles and remains of the wooden beam) was detected on the floor of the structure. The depth of the archaeological deposits is less than 1 m (Senatore *et al.*, 2001).

However, it is still unknown what happened with the remaining houses of the NWI sector. This problem and the need to determine architectural regularities—in size, raw materials and inner divisions—in the houses that are part of the NWI sector, was the objective of an initial geophysical survey during 2000 and a more intensive one in 2001. We applied ground-penetrating radar (GPR) and resistivity methods to characterize the structures and the electromagnetic induction method (EMI) to obtain more information about the inner layers. The analysis of the data revealed a number of anomalies, which, after correlation with the archaeological excavations, could be associated to adobes or similar raw-material walls. These anomalies presented a degree of regularity which should indicate that the NWI sector corresponds to a main structure divided into substructures, each one separated by inner and narrower walls. The data

acquired at the NWI sector were quite different to that of the SWII sector, where a roof collapse had been detected from the excavations (Lascano *et al.*, 2003).

Although a detailed characterization of the NWI sector was achieved, many uncertainties in the interpretation of the anomalies remain. In some cases they could not be interpreted by using inversion methods. In order to aid the interpretation, we study the electric and electromagnetic responses of different structures by using forward-modelling methods (GPR and geo-electric method). We use geophysical data as well as information from excavations as a starting point for modelling the response of different structural features. Moreover, we determine the resolution of both methods to detect different distribution and localization of buried walls. Finally, we correlate the theoretical results to the data in order to obtain a better interpretation of the anomalies and improve the resolution of future geophysical surveys.

Geophysical data

Lascano *et al.* (2003) report the results obtained at the Floridablanca 2001 geophysical campaign. As stated previously, we performed GPR and geo-electrical profiles. The radar data were obtained using a GSSI equipment with a 500 MHz antenna; 12 scans per metre were acquired for each profile, with a scanning time of 60 ns (it can be assumed that the radar is static when measuring). The geo-electric surveys were performed using dipole–dipole configuration with electrode apertures of 0.5 and 0.8 m for the perpendicular and longitudinal profiles respectively. The maximum separation corresponds to $n = 9$.

In Figure 1 we show the location of the radar profiles together with a scheme of the NWI sector (from Lascano *et al.*, 2003, figure 8). The analysis of the radargrams parallel to the axis of the structure show the presence of anomalies only in the profiles located over the mound (lines F30, F31 and F40). An example is shown in Figure 2a, where the radargram corresponding to line F40 is displayed. The anomalies found in those profiles are located at the same depth. The corresponding

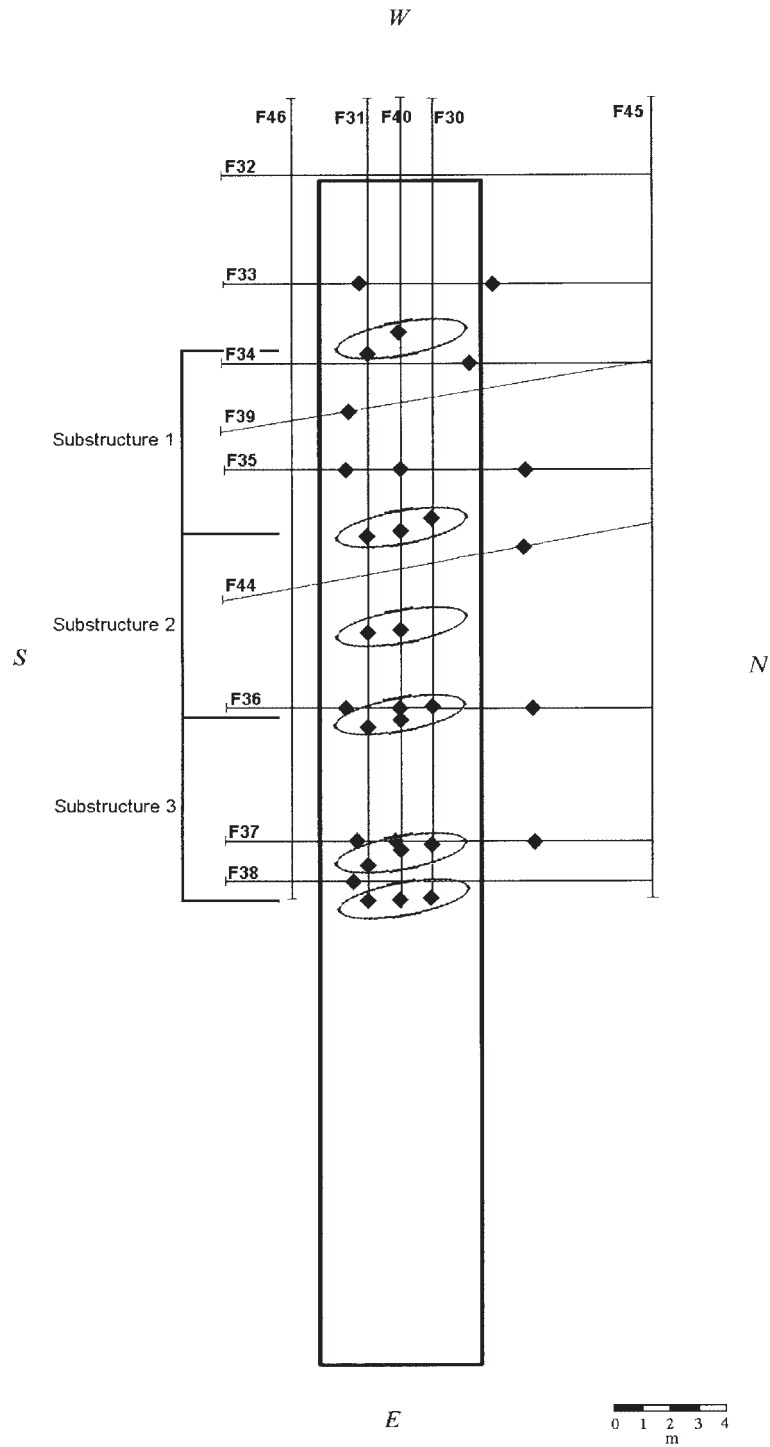


Figure 1. Scheme of the NWI subsector with the radar profiles indicated and the anomalies marked (from Lascano *et al.*, 2003). Also, the substructures delimited by the anomalies are indicated.

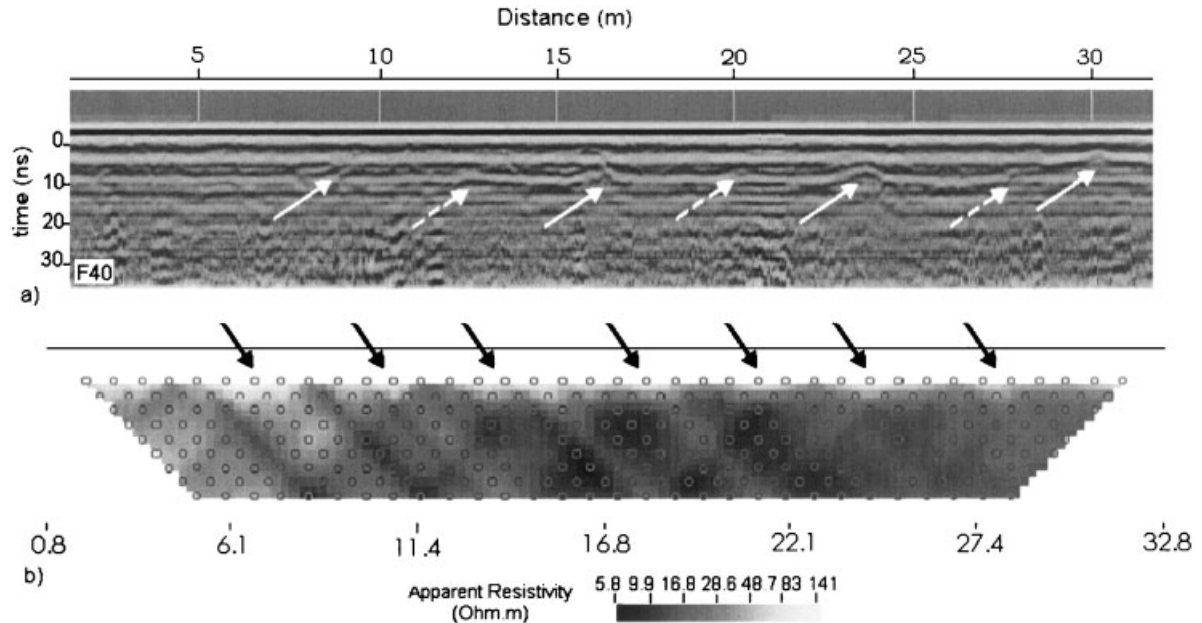


Figure 2. (a) GPR profile F40 and (b) apparent resistivity pseudosection AN5. The white arrows indicate the radar anomalies (full lines, stronger anomalies; dashed lines, weaker anomalies) and the black arrows indicate the resistivity anomalies.

structures do not have a high contrast with the surrounding media, have a similar shape and show a periodic distribution. The anomalies shown in Figure 2a are located at approximately 9, 12, 16, 20, 23, 28 and 30 m (horizontal distance), and at a recording time of 5 ns. Two types of anomalies can be distinguished: a strong one (marked with white arrows) and a weak one (marked with dashed arrows). The difference in strength may indicate the presence of different types of walls: separation walls (strong anomalies) and inner walls (weak anomalies). The separation between the strong anomalies (located at 9, 16, 23 and 30 m, approximately) can be estimated as 7 m. All the profiles present the same behaviour, except that the anomalies are shifted from one profile to the other, which may indicate that the profiles are not perpendicular to the main structure. The weak anomaly seen in Figure 2a at 12 m is present only in this radargram.

The anomalies observed in the perpendicular profiles (F37, F36, F35, F39 and F33) have the same depth and shape than the ones observed in the parallel profiles, indicating that the structures generating these anomalies are similar to those

of Figure 2a. The results are summarized in Figure 1. There is a clear correspondence among the anomalies found in all the profiles. The possible dividing and inner walls are grouped. Three substructures, delimited by the stronger anomalies (separating walls) can be observed. Although the size of the substructures is similar, the internal distribution seems to vary from one substructure to the other. In substructure 1, there is no weak anomaly (inner wall). In substructure 2, the weak anomaly is located 3 m apart from the nearest separation wall, and in substructure 3, the weak anomaly is located 2 m apart from the nearest anomaly. The anomalies found at approximately 5 and 11 m in most of the perpendicular GPR profiles could be the external walls of the houses.

The geoelectrical profiles also present interesting results. In the parallel line AN5 (coincident with F40, see Figure 1), resistive structures down to a depth of 1.5 m are clearly detected, and an apparent periodic pattern is observed below these structures (Figure 2b). As can be seen, the location of these anomalies coincides with those observed in the corresponding radargram. The other resistivity profile AN6 (coincident with F45),

which is located outside the mound, presents a quite homogeneous behaviour.

The excavations carried out in sector SWII show evidence of a layer containing tiles, of approximately 40 cm thickness. To investigate the response of this layer, both GPR and geoelectrical data were acquired along profiles parallel and perpendicular to the SWII sector. Figure 3 shows the comparison between the radargrams acquired in the SWII (Figure 3a) and NWI (Figure 3b) sectors, respectively. The different behaviour of the two responses can be seen clearly. The NWI profile shows a rather uniform behaviour except for the anomalies previously discussed. In contrast, the SWII profile shows a discontinuous response. This difference can be due to the absence of tiles in sector NWI. A similar conclusion is inferred from the geoelectrical pseudosections acquired at both sectors.

Summarizing these results, it can be concluded that the anomalies found with both methods can be due to different kinds of buried structures (adobe walls). Nevertheless, many questions remain unsolved. For example, it is not clear if the differences between the electrical anomalies

correspond to different types of walls and if the different characteristics of the radargrams in the NWI and the SWII sectors are due to the absence and presence of tiles, respectively. Other uncertainties concern the characterization of collapsed walls and the resolution of thin walls. In the following, we use numerical simulation of GPR and geoelectrical responses to improve the interpretation.

Modelling

Radargrams

The radar simulations are based on the forward modelling code developed by Carcione (1996a–c) using the Fourier pseudospectral method. The simulations use a numerical mesh of 1080×160 grid points, with a grid spacing of 1 cm (20 grid points at the sides and bottom of the mesh are used to absorb the wave field exiting the model). The source is a Ricker-type wavelet with a dominant frequency of 500 MHz, applied as a vertically propagating plane wave to approximate a monostatic survey as it was done in the field. The

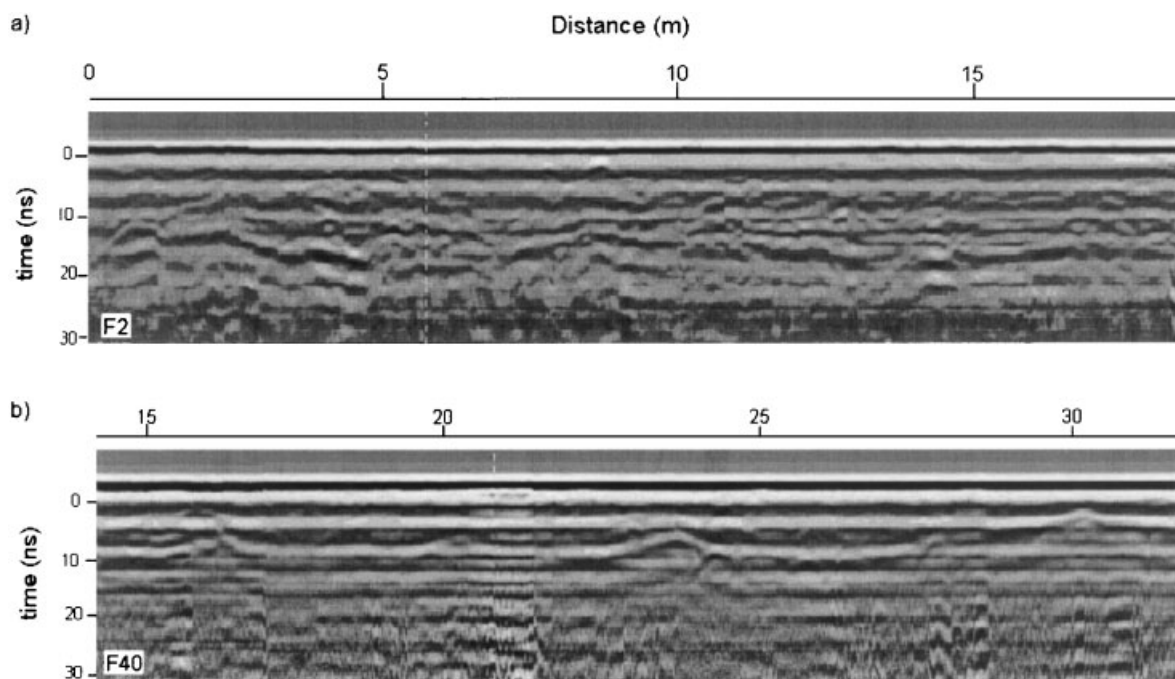


Figure 3. (a) Parallel profile acquired in the SWII sector, and (b) parallel profile acquired in the NWI sector.

source is located at the air–soil interface and has horizontal polarization. The two-dimensional numerical modelling algorithm uses a time step of 0.01 ns.

Electrical tomographies

The geoelectrical simulation is performed with the DCIP2D (2000) program developed by the University of British Columbia and based on the work of Oldenburg *et al.* (1993) and Oldenburg and Li (1994). This program computes DC potentials by means of a finite-difference technique, and we use a numerical mesh of 106×34 grid points, with a grid spacing of 20 cm. The dipole–dipole configuration is used with an electrode aperture of 0.8 m.

Electrical model

The model is obtained from the information provided by the inversion of the geoelectrical profiles (Lascano *et al.*, 2003): a sedimentary layer of 85 cm thickness, formed by clayed sand with relative permittivity equal to 4 and conductivity equal to 0.02 S m^{-1} , and below it, a layer of wet clay with relative permittivity equal to 10 and conductivity equal to 0.1 S m^{-1} . The adobe walls are embedded in the sedimentary layer at a depth of 12 cm and the height of these walls is 60 cm. We simulate the major walls, constituting the house boundaries (separation walls), as blocks of 40 cm width, and a minor block of 20 cm width is used to represent the inner walls. In both cases, the blocks have a relative permittivity equal to 2 and conductivity equal to 0.003 S m^{-1} . The values of the conductivities correspond to those of Lascano *et al.* (2003) and the values of the permittivities can be found in Daniels (1996) and Perez Gracia *et al.* (2000).

The models used for the numerical simulations are inferred from the sequence of anomalies observed in Figure 2 and summarized in Figure 1. First, we model substructure 2 as two inner walls 7 m apart with an inner thinner wall located 3 m from one of the walls (case A). The results are then applied to interpret substructure 3, where the inner wall is 1 m from one of the main walls. Then, we study the responses by assuming that the middle wall has

collapsed to the left side (case B), that the height of the middle wall has been halved (case C) and that the inner wall is not present (case D). These last three cases are proposed to explain the different intensity, absence and/or shift of the weaker anomaly in both the GPR and the geoelectrical profiles, in order to define substructure 1. We also introduce random noise in the models, which could be responsible for ‘hiding’ the separation walls. To complete the analysis, two more simulations are performed to analyse the radargram and apparent resistivity when more resolution is required. These simulations are similar to those of cases B and C, but with a dominant frequency of 1 GHz for the GPR simulations and an electrode separation of 0.5 m for the resistivity simulations.

Finally, we estimate the effect of the tiles due to the roof collapse, simulating two cases: a highly resistive layer of $800 \Omega\text{m}$ located between the walls, and blocks of 40 cm width, 10 cm height and a resistivity of $800 \Omega\text{m}$, but randomly distributed between the walls (case E).

Results

Case A: two separation walls 7 m apart and an internal wall at 3 m to the left of one of the separation walls. The separation walls are centered at $x = 3.2 \text{ m}$ and $x = 10.2 \text{ m}$, and the inner wall at $x = 7.1 \text{ m}$, respectively.

The synthetic radargram is shown in Figure 4a. We observe the direct wave till approximately 2 ns, the reflected wave from the sand–clay interface at approximately 14 ns, and the responses of the walls at the expected horizontal locations. The diffraction-reflection hyperbolae generated by the top and bottom of the walls are clear at 4 ns and between 8 and 13 ns, respectively. Note the dissimilar responses for different wall widths. The attenuation versus depth is greater for the thinner wall. At the location of the walls, the reflection from the sand–clay interface arrives in advance, owing to the higher electromagnetic velocity of the walls compared with that of the sand.

In Figure 4b, the anomalies generated by each buried wall can be seen clearly as higher apparent resistivity values. The shape of the anomalies

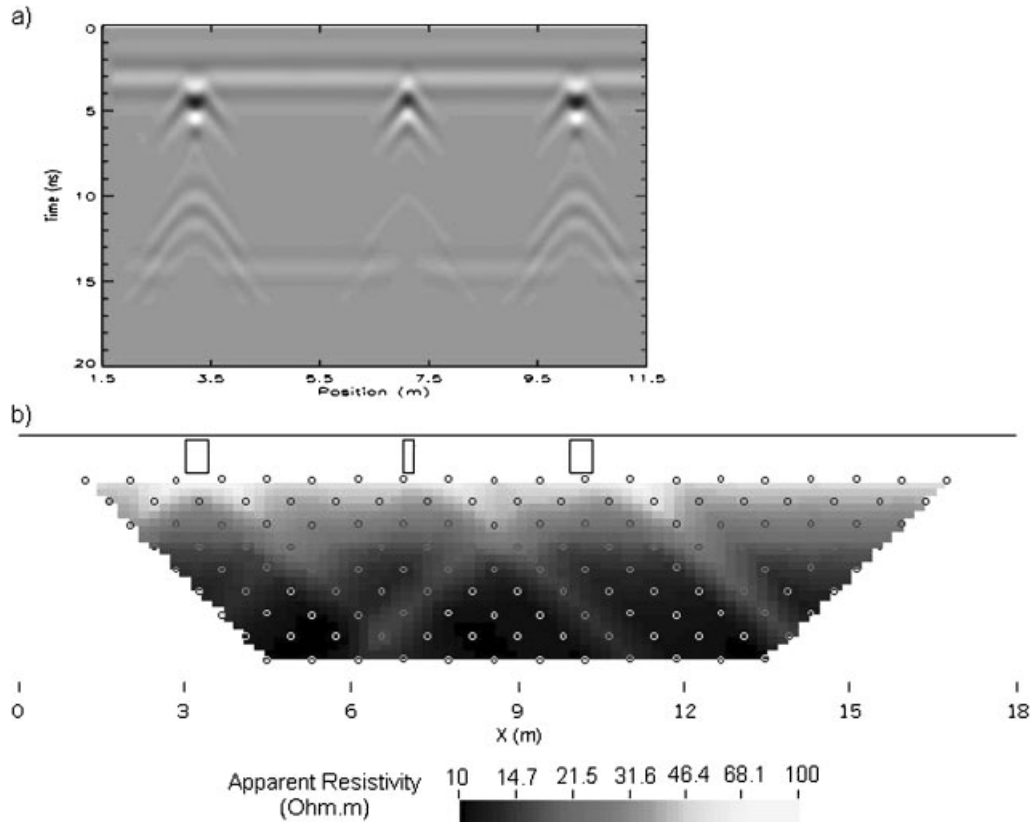


Figure 4. Case A simulation: (a) synthetic radargram; (b) modelled resistivity pseudosection. The blocks indicate the location of the walls.

is not the same for identical walls, because it depends on the relative position of the electrodes and the wall. As expected, the wider walls (separation walls) present a stronger anomaly than the inner wall. For both, the inner and the external wall at the right-hand side, the anomaly is shifted between 0.8 and 1.6 m from the actual position of the wall. The presence of the buried walls also can be detected from the deeper points of the profile. The uniform conductive layer (apparent resistivity of approximately $10 \Omega\text{m}$) is interrupted by more resistive points aligned along inclined lines (apparent resistivity of approximately $15 \Omega\text{m}$) that form an inverted V underneath each wall.

Case B: two separation walls 7 m apart, and the inner wall collapsed to the left-hand side.

The synthetic radargram is shown in Figure 5a. The external walls have a similar response as in

the previous case. The collapsed wall, modelled as a block of 20 cm height and 60 cm width, presents a wider response and can be seen after 9 ns. Figure 5b shows the apparent-resistivity simulation corresponding to case B. The response of the collapsed inner wall is not clear because the anomaly and contrast with the surrounding medium are much weaker than in case A.

Case C: two separation walls 7 m apart, and the height of the middle wall has been halved.

In this case, the height of the inner wall is 30 cm, instead of 60 cm. The difference of the corresponding radargram (Figure 6a) compared with that obtained for the collapsed wall is clear, both in the location of the top of the reflection hyperbola (approximately 7 ns) and in its width. Although there is only a difference of 10 cm between the height of the collapsed wall

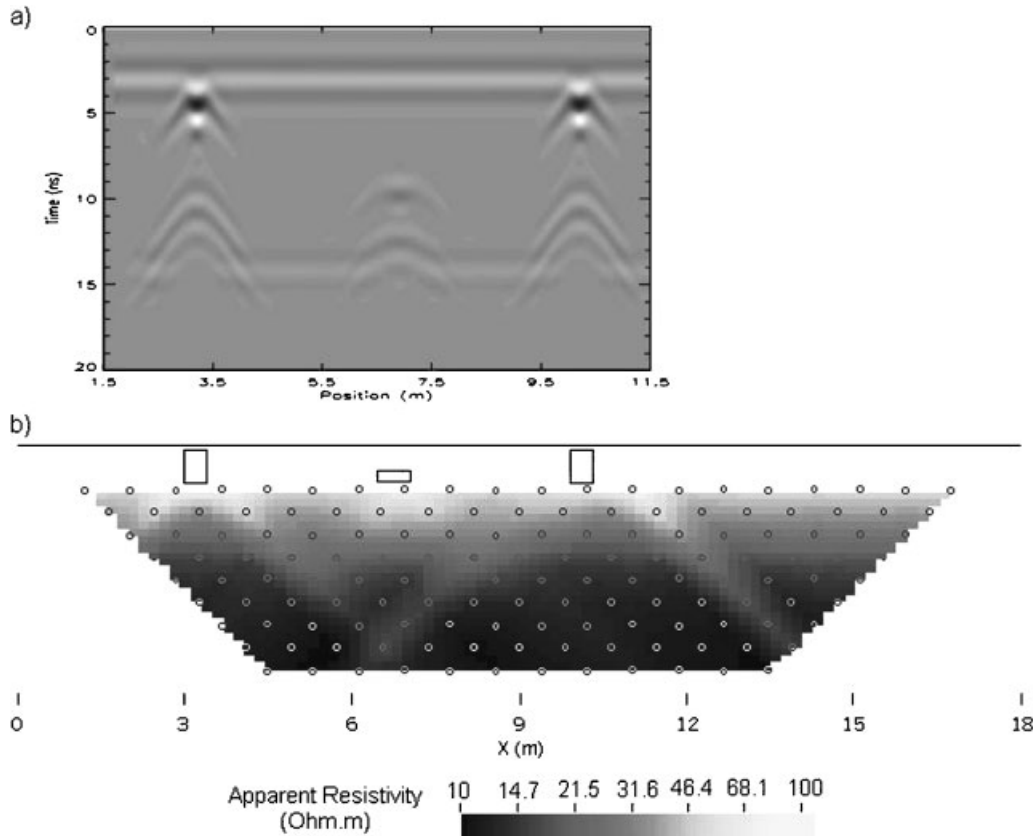


Figure 5. Case B simulation: (a) synthetic radargram; (b) modelled resistivity pseudosection. The blocks indicate the location of the walls.

(20 cm) and this case (wall of 30 cm height), the time shift of the anomaly can be appreciated in the synthetic radargram. The geo-electric simulation (Figure 6b) shows that in this case the wall cannot be resolved, so a shorter wall cannot be detected, at least with the electrode aperture used in this simulation.

Case D: two separation walls 7 m apart from each other and no inner wall.

We observe a similar response, regarding the external walls, to that of the previous cases (so we do not show them here). As no interference in the region between them appeared in GPR, the presence or absence of an inner wall could be determined. In contrast, we could not distinguish from the dipole-dipole profiles if there is a halved or collapsed wall or if there is no inner wall at all.

We improved the resolution for cases B and C assuming a 1 GHz antenna and electrode separa-

tion of 0.5 m. The corresponding radargrams revealed a better resolution for the first reflections, especially in the definition of the vertical dimension of the walls, but the attenuation is larger for cases B and C. The apparent resistivity profiles for both cases are, as expected, clearer than for an electrode aperture of 0.8 m. Despite this fact, this electrode aperture does not improve very much the resolution of the profile and the inner wall remains unseen by the configuration. Also, the lower conductive layer is not well defined. So, although this electrode aperture allows us to distinguish the buried walls more clearly, we cannot obtain information about the medium where the buried structures are embedded.

We also evaluated the effect produced by actual data adding different levels of noise. We tried up to 30% of random noise, which could take into account different sources (cultural,

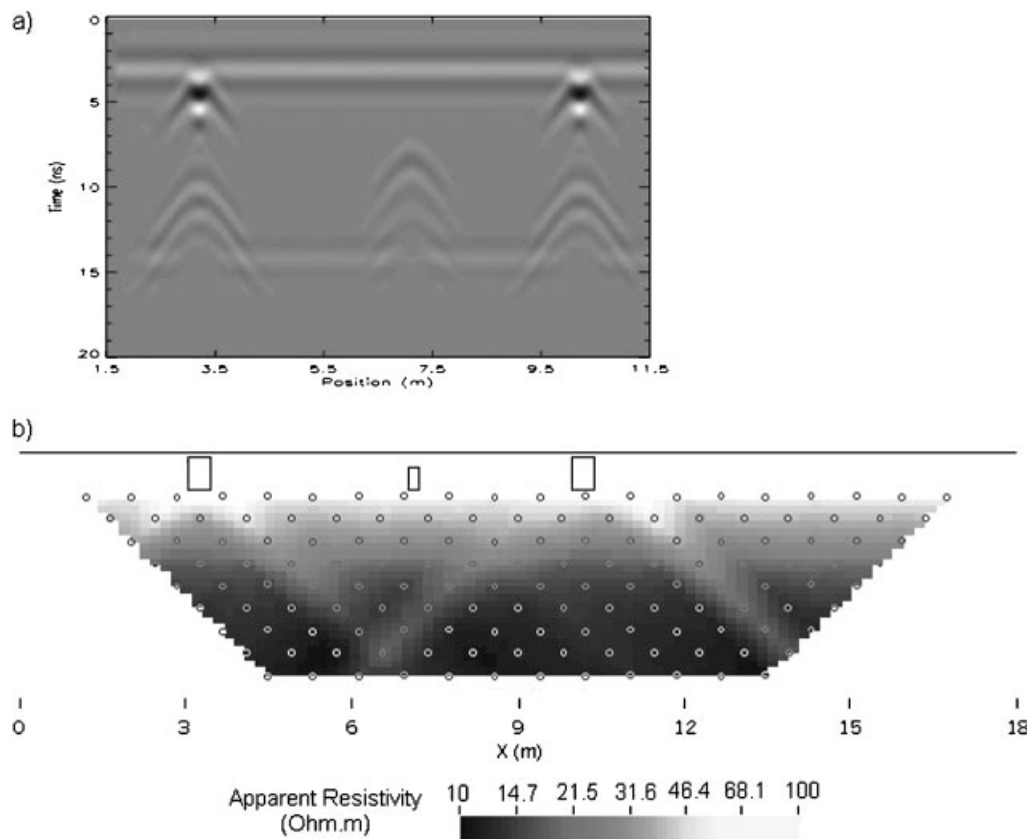


Figure 6. Case C simulation: (a) synthetic radargram; (b) modelled resistivity pseudosection. The blocks indicate the location of the walls.

geological, instrumental) with no detectable effect on the responses.

Case E: including a layer simulating tiles.

We introduce a collapsed roof between the walls in two different ways: as a uniform resistive layer 40 cm thick and as uniform resistive blocks distributed randomly between the walls. In the first case, the response of the model does not present any similarity with the data. In contrast, the simulation of the second case reproduces the GPR data as shown in Figure 7a. The response of the top of the walls is visible, but the response of the bottom is lost. The tiles are characterized by a non-uniform response between the walls. In Figure 7b, the geo-electrical forward modelling corresponding to the radargram is shown. The tiles manifest themselves as higher values of apparent resistivity between the walls, but the walls cannot be distinguished. Because of this, we study the same model with

a higher resolution. In Figure 7c, the geo-electrical forward modelling using electrode apertures of 0.5 m is shown. In this case, the tiles also manifest themselves with high values of apparent resistivity, but the walls can be distinguished by the inclined high apparent resistivity lines underneath them.

Discussion and conclusions

As a first step in data interpretation (Lascano *et al.*, 2003), the boundaries of three substructures corresponding to the NWI sector were defined by taking into account the archaeological information available. These substructures could be the houses of the dwellers of the Floridablanca Colony. Different anomaly distributions were found inside each of these substructures indicating a possible different internal organization of

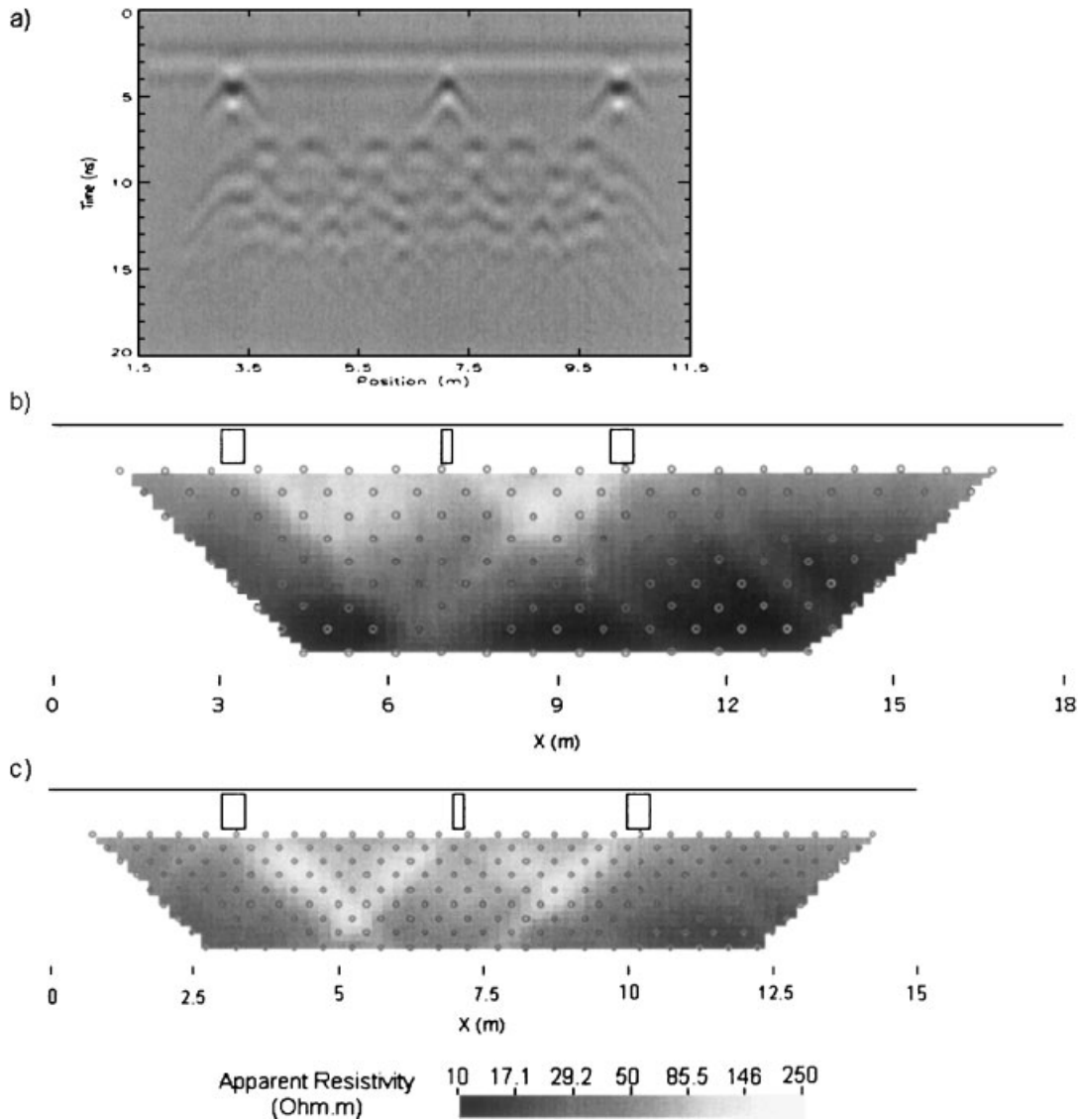


Figure 7. Case E simulation, modelling tiles as uniform blocks distributed randomly between the walls. (a) Synthetic radargram. Modelled resistivity pseudosection with electrode aperture of (b) 0.8 m and (c) 0.5 m.

the houses. From an archaeological point of view, this is an important issue to study.

The anomalies produced by our target archaeological structures were very weak because they presented similar electromagnetic properties to the surrounding soil. Hence, they could not be recovered with inversion methods. Regarding the GPR data, weak anomalies could be confused with irregularities; also, they may not be resolved with inversion techniques using the geoelectrical method. Having this in mind, the objective of this

paper was to resolve these ambiguities by using forward modelling methods. We have obtained the responses of different geometrical distributions of the buried structures. These synthetic responses obtained from the numerical simulations have been used to identify the anomalies and to recognize them both in the geoelectrical and GPR real data.

Different structures have been simulated to model the adobe walls, according to the anomalies detected at each substructure (Figure 1). The

results obtained from the simulation of GPR and geo-electrical responses indicated that the walls can be differentiated despite the low resistivity contrast with the surrounding media. Some limitations, however, appeared when making comparison with real data, in particular because there is a clear difference between the real and synthetic radargrams, thus reducing the sensitivity to distinguish some of the cases.

Case A was meant to resemble the anomalies distribution found at substructures 2 and 3 (see Figure 1). The geoelectrical forward model (Figure 4b) presents the same anomaly distribution, both in shape and location, as in the real data (Figure 2b). The sensitivity is enough to distinguish between the inner and major walls, and can be improved by decreasing the electrode apertures. In this case, the lower aperture implies lower penetration; then a combined geometry should be used to produce better lateral resolution with deep penetration. Regarding the GPR data, the attenuation of the signal plus the noise produced by the medium inhomogeneities, screen the scattering produced by the base of the walls. Because of this, only the upper part of the walls is detected in the data, coinciding also in shape and location with the synthetic responses (Figures 2a and 4a, respectively). From these results, we can confirm that substructure 2 corresponds to a house delimited by two separation walls (strong anomalies) with an inner thinner wall (weak anomaly) located at approximately 3 m from one of the main walls. In contrast, the inner wall in substructure 3 is closer to one of the separating walls, at about 1 m. The differences in the internal organization of the houses is a matter of archaeological interpretation.

Case B and C were performed to interpret the pattern found at substructure 1, where there is no weak anomaly indicating the presence of an inner wall (see Figure 1). A possible explanation could be that the inner wall could be halved or collapsed. The geoelectrical forward modelling indicates that in none of these cases the inner wall can be resolved (see Figures 5b and 6b, respectively), even if the resolution is improved by decreasing the electrode separation. Regarding the GPR responses, the synthetic radargrams indicate that both types of situa-

tions could be distinguished due to the time shift and width of the anomaly (Figures 5a and 6a, respectively). However, the limitations appeared when comparing with the real data (Figure 2a). The real signal attenuates with depth, and the top of the reflection hyperbola corresponding to the inner wall is screened. So, the absence of a weak anomaly in substructure 1 means that there is not an intact inner wall, as in substructure 2, but there could be a halved or collapsed one. Moreover, if we take into account the screening in the real radargrams, the results from case D (no inner wall inside) cannot be disregarded. In this case, the characteristics of substructure 1 cannot be completely resolved and the inner distribution remains ambiguous.

Another interesting result, shown in Figure 7, is that the presence and absence of tiles can be distinguished clearly. Comparing with data, it can be established that there is no evidence of roof collapses along this structure. This is a very interesting result from the archaeological point of view, as it indicates that this structure has not been finished, and then, the houses were not inhabited.

Summarizing the results, we conclude that forward-modelling techniques allow us to improve the interpretation of the data, which in turn results in a better plan for further archaeological excavations.

Acknowledgments

This work was partially supported by ANPCyT (Agencia Nacional de Promoción Científica y Tecnológica) and MAE (Ministero degli Affari Esteri, Italia).

References

- Carcione JM. 1996a. Ground penetrating radar: wave theory and numerical simulation in lossy anisotropic media. *Geophysics* **61**: 1664–1677.
- Carcione JM. 1996b. Ground radar simulation for archaeological applications. *Geophysical Prospection* **44**: 871–888.
- Carcione JM. 1996c. Ground-radar numerical modelling applied to engineering problems. *European Journal of Environmental and Engineering Geophysics* **1**: 65–81.

- Carrara MT. 1996. Santa Fe La Vieja, primer enclave urbano en el corredor paranaense. *Jornadas de Antropología de la Cuenca del Plata II*: 135–146. (Facultad de Humanidades y Arte, Escuela de Antropología, UNR).
- Daniels DJ. 1996. Surface-penetrating radar. *IEE Radar, Sonar, Navigation and Avionics Series 6*.
- DCIP2D. 2000. *Forward Modelling and Inversion of DC Resistivity and Induced Polarization Data over 2D Structures*, V3.2. Geophysical Inversion Facility, University of British Columbia.
- Herbich T, Misiewicz K, Teschauer O. 1997. Multi-level resistivity prospecting of architectural remains: the Schwarzach case study. *Archaeological Prospection 4*: 105–112.
- Lascano E, Osella A, de la Vega M, Buscaglia S, Senatore X, Lanata JL. 2003. Geophysical prospecting at Floridablanca archaeological site, San Julián Bay, Argentina. *Archaeological Prospection 10*: 1–18.
- Oldenburg DW, Li Y. 1994. Inversion of induced polarization data. *Geophysics 59*: 1327–1341.
- Oldenburg DW, McGillivray PR, Ellis RG. 1993. Generalized subspace method for large scale inverse problems. *Geophysical Journal International 114*: 12–20.
- Pérez Gracia V, Canas JA, Pujades LG, Clapés J, Caselles O, Gracia F, Osorio R. 2000. GPR survey to confirm the location of ancient structures under the Valencian Cathedral (Spain). *Journal of Applied Geophysics 43*: 167–174.
- Ponti N, Fanton G, Imhof A, Pastore S. 1996. Investigaciones geoelectricas con fines arqueológicos en Santa Fe La Vieja, Provincia de Santa Fe, República Argentina. *Jornadas de Antropología de la Cuenca del Plata II*: 128–130. (Facultad de Humanidades y Arte, Escuela de Antropología, UNR).
- Senatore MX. 2000. Arqueología en Floridablanca, Provincia de Santa Cruz. *Anales de la Academia Nacional de Ciencias de Buenos Aires XXXIV*(2): 743–753.
- Senatore MX, Cardillo M, Bianchi Vilelli M, Buscaglia S. 2000. Arqueología en Floridablanca. Primeros Resultados. In *Actas del IIIer Congreso de Americanistas*, Sociedad Argentina de Americanistas, Universidad del Salvador; 201–225.
- Senatore MX, Bianchi Vilelli M, Buscaglia S, Marschoff M. 2001. Hacia la definición del plano arqueológico del enclave españoles de Floridablanca en San Julián. *Relaciones XXXVI*: 323–344.
- Silliman SW, Farnsworth P, Lighfoot KG. 2000. Magnetometer prospecting in historical archaeology: evaluating survey options at 19th-century Rancho Site in California. *Historical Archaeology 34*(2): 89–109.
- Weston DG. 2001. Research notes. Alluvium and geophysical prospecting. *Archaeological Prospection 8*: 265–272.